

IL6Myc mouse is an immunocompetent model for the development of aggressive multiple myeloma

Michael D. Pisano,^{1,2} Fumou Sun,³ Yan Cheng,³ Deepak Parashar,² Vivian Zhou,² Xuefang Jing,⁴ Ramakrishna Sompallae,⁵ Jenica Abrudan,⁶ Michael T. Zimmermann,⁶ Angela Mathison,⁶ Siegfried Janz² and Miles A. Pufall⁷

¹Interdisciplinary Graduate Program in Immunology, University of Iowa, Iowa City, IA; ²Division of Hematology and Oncology, Department of Medicine, Medical College of Wisconsin, Milwaukee, WI; ³Myeloma Center, Department of Internal Medicine and Winthrop P. Rockefeller Cancer Institute, University of Arkansas for Medical Sciences, Little Rock, AR; ⁴Department of Pathology, University of Iowa Roy J. and Lucille A. Carver College of Medicine, Iowa City, IA; ⁵Iowa Institute for Genetics, University of Iowa Roy J. and Lucille A. Carver College of Medicine, Iowa City, IA; ⁶Genomic Sciences and Precision Medicine Center, Medical College of Wisconsin, Milwaukee, WI and ⁷Department of Biochemistry and Molecular Biology, the University of Iowa Roy J. and Lucille A. Carver College of Medicine, Holden Comprehensive Cancer Center, Iowa City, IA, USA

Correspondence: M.A. Pufall
mpufall@uiowa.edu

Received: December 12, 2022.

Accepted: July 4, 2023.

Early view: July 13, 2023.

<https://doi.org/10.3324/haematol.2022.282538>

©2023 Ferrata Storti Foundation

Published under a CC BY-NC license



Abstract

Multiple Myeloma (MM) is a plasma cell neoplasm originating in the bone marrow and is the second most common blood cancer in the United States. One challenge in understanding the pathogenesis of MM and improving treatment is a lack of immunocompetent mouse models. We previously developed the IL6Myc mouse that generates plasmacytomas at 100% penetrance that phenotypically resemble aggressive MM. Using comprehensive genomic analysis, we found that the IL6Myc tumors resemble aggressive MM by RNA and protein expression. We also found that IL6Myc tumors accumulated fusions and missense mutations in genes that overlap significantly with human myeloma, indicating that the mouse is good model for studying disease etiology. Lastly, we derived cell lines from IL6Myc tumors that express cell surface markers typical of MM and readily engraft into mice, home to the bone marrow, and induce osteolytic disease. The cell lines may be useful in developing immunotherapies directed against BAFF-R and TACI, though not BCMA, and may also be a good model for studying dexamethasone resistance. These data indicate that the IL6Myc model is useful for studying development of aggressive MM and for developing new treatments against such forms of the disease.

Introduction

Multiple myeloma (MM) is the second most common hematological malignancy in the United States. Although immunotherapies show promise in curing MM, most patients receive conventional treatments that are temporary in efficacy and subject to eventual relapse with more aggressive disease¹⁻³ Better treatments are urgently needed. One challenge in developing new treatments is the availability of MM models. Several mouse models have been developed, two of which have come into wide use, Vk*MyC and 5TMM,^{4,5} that faithfully recapitulate aspects of the disease. Both models are immunocompetent but are driven differently: Vk*MyC by relying on AID-dependent activation of Myc⁴ and 5TMM by relying on transfer of a 5T cell line to C57BL/KaLwRij mice.^{4,5} Both models have made important progress in addressing the role of the immune system in MM. 5TMM models have helped to elucidate the role of the Th1:Th2 axis in MM⁶ and anti-PD-L1

immunotherapy⁷ and Vk*MyC mice have elucidated roles of natural killer (NK) and CD8 T-cell surveillance⁸ and the role of interleukin 17 (IL17), and Th17 cells, in disease progression.⁹ The 5TMM models of MM have proven useful in studying bone marrow homing and myeloma-like bone disease (MBD).¹⁰ The Vk*MyC mouse has also proven useful in tracking gene expression changes that underlie the progression from monoclonal gammopathy of undetermined significance (MGUS) to MM and the accumulation of genetic lesions in the form of copy number variations (CNV) that are associated with disease and intratumoral heterogeneity.¹¹ In addition to helping elucidate the etiology of MM, both models have been useful in developing treatments.

In our laboratory we developed an immunocompetent model that appears to mimic aggressive or high-risk disease; the IL6Myc mouse. Global overexpression of IL6 is a proliferative signal that contributes to the differentiation of B cells into plasma cells. Myc is overexpressed by an

iMycE μ transgene in B cells inserted upstream of the intronic Igh enhancer, which recapitulates the t(8;14)(q24;q32) translocation from Burkitt lymphoma. IL6Myc mice develop plasmacytomas quickly, in 45 to 175 days, with 100% penetrance, with average survival of 91.6 days.¹² Importantly, IL6Myc plasmacytomas phenotypically resemble human MM, including a peripheral blood M-spike,¹² lytic bone disease, and malignant plasma cell infiltration in the peripheral lymph nodes, kidney, and liver.^{13,14} The development of extramedullary disease in the spleen and mesenteric lymph nodes that is characteristic of the IL6Myc mouse is rare in MM, but is associated with MM patients that have progressed to plasma cell leukemia.¹⁵ M-spikes in IL6Myc mice are initially more oligoclonal, in contrast with monoclonal disease observed in human MM, but become less polyclonal as the mice age.¹³ The striking penetrance, consistency, and phenotypic resemblance to aggressive MM disease suggest that the IL6Myc mouse is a useful model for testing treatments and studying MM development.

One model for MM development is *Myc* addiction. *Myc* variants occur in >40% of newly diagnosed myelomas, with *Myc* overexpressed in 67% of frank MM.¹⁶ This suggests that *Myc* expression sets the conditions for MM development as B cells become “addicted to *Myc*”.¹⁷ *Myc* overexpression alone is insufficient to drive myelomagenesis, indicating that other genetic lesions are required for transition to MM. Expression of IL6 and *Myc* may provide the conditions, as in the Vk**Myc* mouse, to accumulate gene variants that drive development of aggressive MM.⁴ In order to molecularly characterize the IL6Myc mouse, and to determine which clinical subtype(s) IL6Myc most resembles we conducted comprehensive genomic profiling. In order to determine which malignancies IL6Myc tumors most resemble and to identify genes/proteins that are potentially driving the disease, we performed RNA sequencing (RNA-seq) and reverse phase protein arrays (RPPA). In order to determine whether the IL6Myc mouse generates genetic lesions that are consistent with development of MM we analyzed RNA-seq data for gene fusions and performed whole-exome sequencing (WES) to identify protein-coding mutations. Lastly, inspired by the generation of 5T cells, we derived IL6Myc cell lines which we characterized for engraftment, homing, cell surface markers, and drug sensitivity to determine their suitability for developing models to test better treatments.

Methods

Mice

IL6Myc mice were bred by crossing BALB/c.IL6 and iMyc^{E μ} mice as described previously. Experiments conducted under MCW Animal Use Application #AUA00006541.

RNA sequencing

IL6Myc tumor, naïve, and activated B cells were isolated, RNA extracted (Qiagen RNeasy) from specimens, sequenced, processed (TrimGalore), and mapped (Salmon), gene set enrichment analysis (GSEA), and subjected to fusion gene analysis (STAR-Fusion). Principal component analysis (PCA), similarity, and differential gene expression (DESeq2) were conducted in RStudio 4.1.1 (see attached KnitScript.pdf). Quantitative polymerase chain reaction (qPCR) was performed using iScript™ and SYBR® Green Master Mix (Bio-Rad).

Reverse-phase proteomic array

Forty-four mouse MLN tumors and three wild-type (WT) splenic B cells were isolated from BALB/c and analyzed by the MD Anderson Functional Proteomics RPPA Facility as described previously.¹⁸ Reverse-phase proteomic array (RPPA) data was further analyzed in R.

Whole-exome sequencing

DNA was extracted from 45 IL6Myc MLN tumor samples and five BALB/c Kidney samples, exonic DNA captured (SureSelectXT Mouse All Exon), sequenced, and analyzed in R/Bioconductor. Overlap between sets of variants was assayed by hypergeometric test.

Derivation of IL6Myc cell lines

IL6Myc cell lines were derived from splenic (IL6Myc-1) and mesenteric lymph node (IL6Myc-2,3,4,5) tumors. Cells were single-cell cloned and cultured in IMDM supplemented plus 15% fetal bovine serum (FBS).

Flow cytometry

Cells were isolated from culture, washed, and blocked with 1 ng/ μ L Fc blocking antibody for 10 minutes (min), incubated with antibodies for 30 min, washed, resuspended in phosphate-buffered saline (PBS) with 2% FBS and run on a BD Accuri™ C6 Plus Flow Cytometer. Data were analyzed using FlowJo.

X-ray microscopy and microtomography imaging of mice with IL6Myc-1 adoptive transfer

IL6Myc-1 cells were engrafted by adoptive transfer. For X-ray microscopy and X-ray microtomography (μ CT) imaging mouse carcasses were fixed in formalin, fit in tubes, and imaged using dual-energy 3D X-ray microscopy (Zeiss Xradia 520 Versa). Projections were collected through 360° rotations. Images were analyzed using the BoneJ (v. 1.3.14, ImageJ v. 1.49 m).

Histological analysis and tartrate-resistant acid phosphatase staining

Bone samples were fixed in formaldehyde, decalcified, rinsed with PBS, fixed in cold 70% ethanol, and embedded

in paraffin. Tissue sections were stained for tartrate-resistant acid phosphatase (TRAP) activity using an acid phosphatase leukocyte kit (Sigma). Specimens were counterstained with eosin and mounted for imaging and histomorphometry. Osteoclasts were enumerated in five high-power microscopy fields per slide.

BAFF and APRIL stimulation

Cells were harvested from culture, seeded at 1×10^5 cells per well in 100 μ L IMDM plus 1% FBS and treated with vehicle (1% FBS IMDM), 100 ng/mL APRIL, or 100 ng/mL BAFF for 72 hours (h). Viability was measured by incubating with MTS reagent and read at 490 nm (SpectraMax i3x).

Drug treatment

Cells were seeded in IMDM plus 15% FBS in 96-well plates. Stocks of drugs were diluted, titrated into wells, and incubated for 24–72 h. Viability was measured by Promega Real-Time Glo reagent with fluorescence (SpectraMax i3x). Data was analyzed using GraphPad Prism.

Results

Gene expression patterns of IL6Myc tumors are similar to human multiple myeloma

In order to determine whether the tumors molecularly resemble human MM, we performed RNA-seq. PCA comparing gene level counts of seven splenic (SPL) and seven mesenteric lymph node (MLN) tumors to five lipopolysaccharide (LPS)-activated (plasmablast) and four quiescent BALB/c B-cell controls showed that the tumors were distinct from controls but did not cluster by mouse or disease location (Figure 1A). PCA followed by centroid analysis of human myeloma, diffuse large B-cell lymphoma (DLBCL), acute myeloid leukemia, acute lymphoblastic leukemia (ALL) and Burkitt lymphoma, as well as prostate cancer and breast cancer downloaded from the Cancer Genome Atlas (TCGA), indicates that IL6Myc tumors most closely resemble MM (Figure 1B). Single-linkage hierarchical clustering (*Online Supplementary Figure S1*) indicated that IL6Myc tumors were most similar to DLBCL, with human MM next. These results indicate that IL6Myc tumors resemble mature B-cell malignancies including MM. In order to determine whether IL6Myc tumors resemble a subtype of MM, we compared IL6Myc tumors to translocation, disease stage and outcome subsets of human MM using RNA-seq data from the Multiple Myeloma Research Foundation (MMRF) CoMMpass database. Although IL6Myc tumors clustered with MM, they did not resemble any specific subtype (*Online Supplementary Figure S2*).

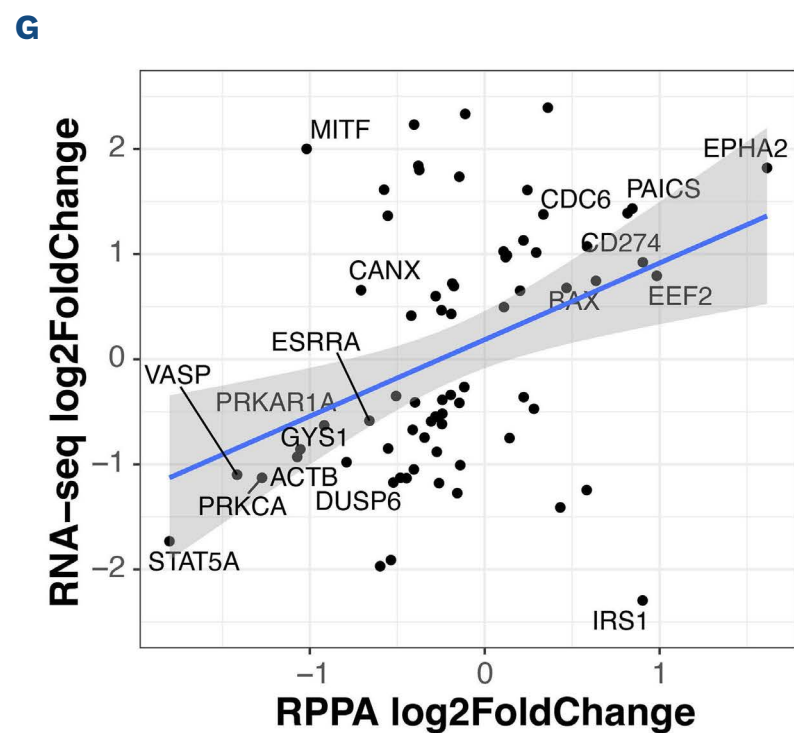
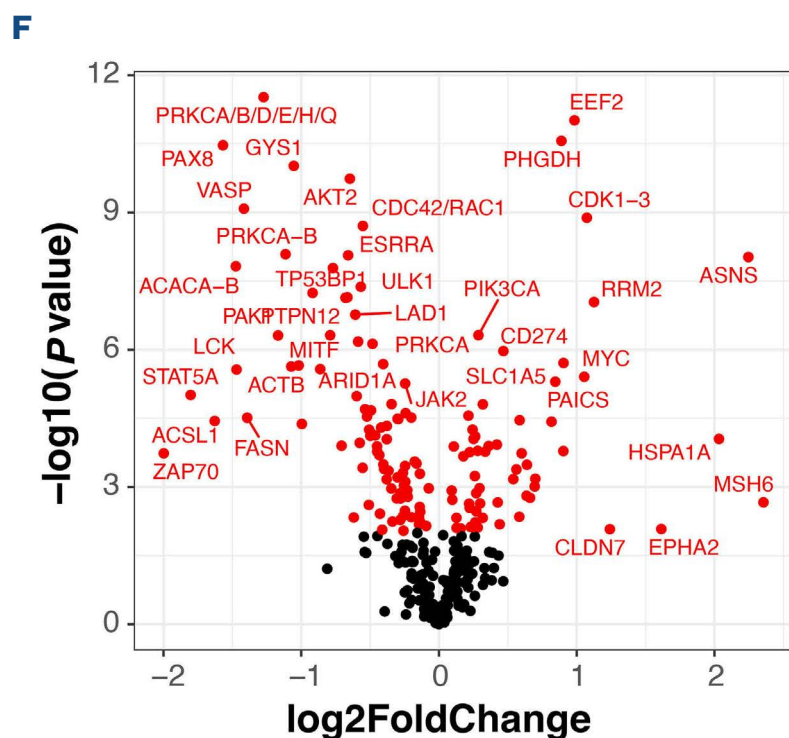
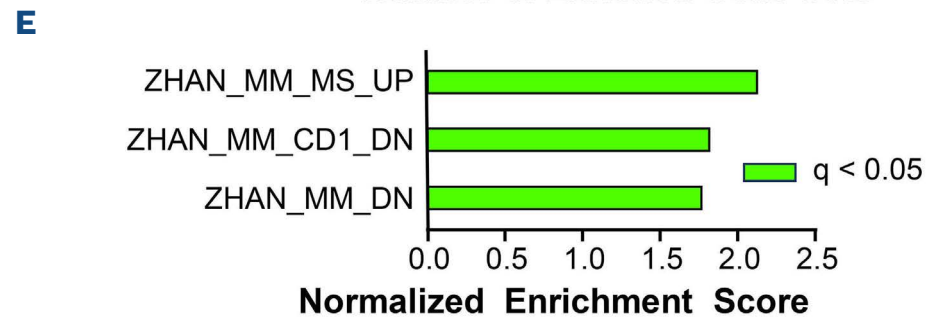
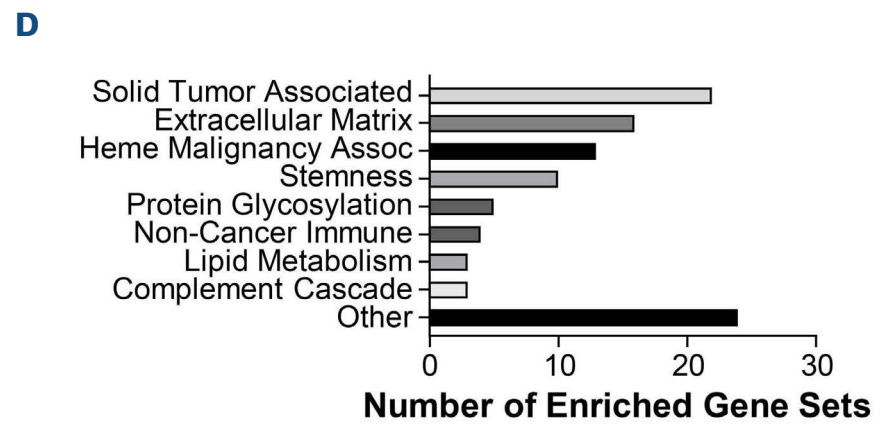
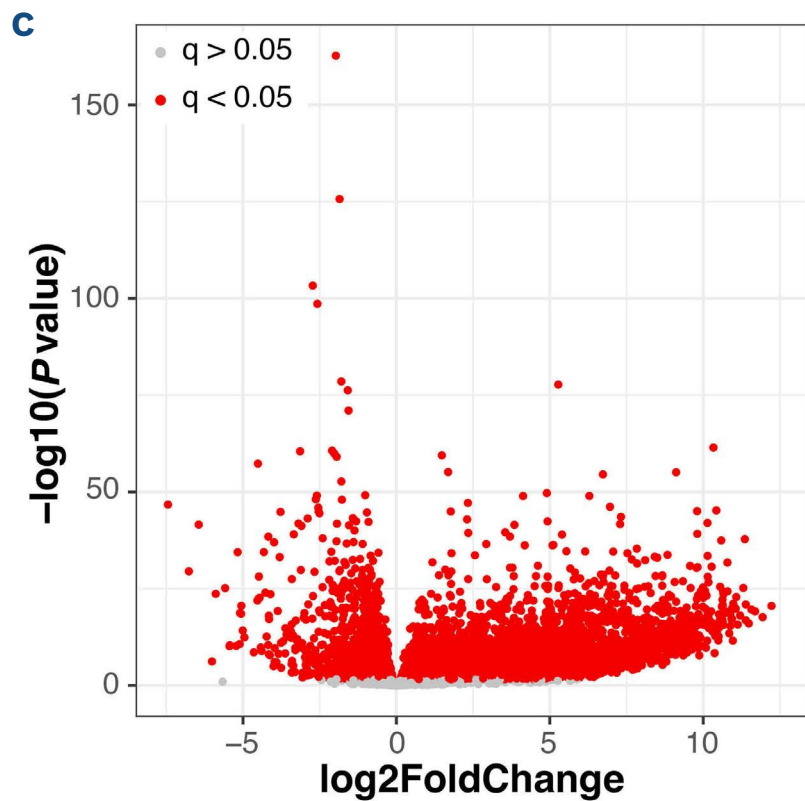
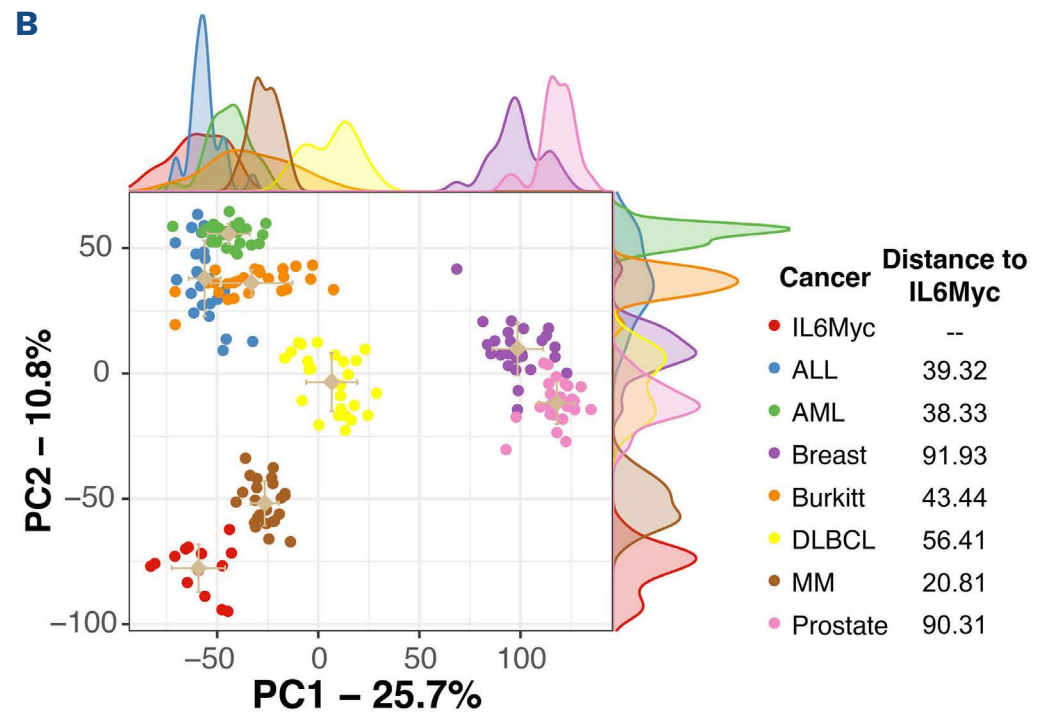
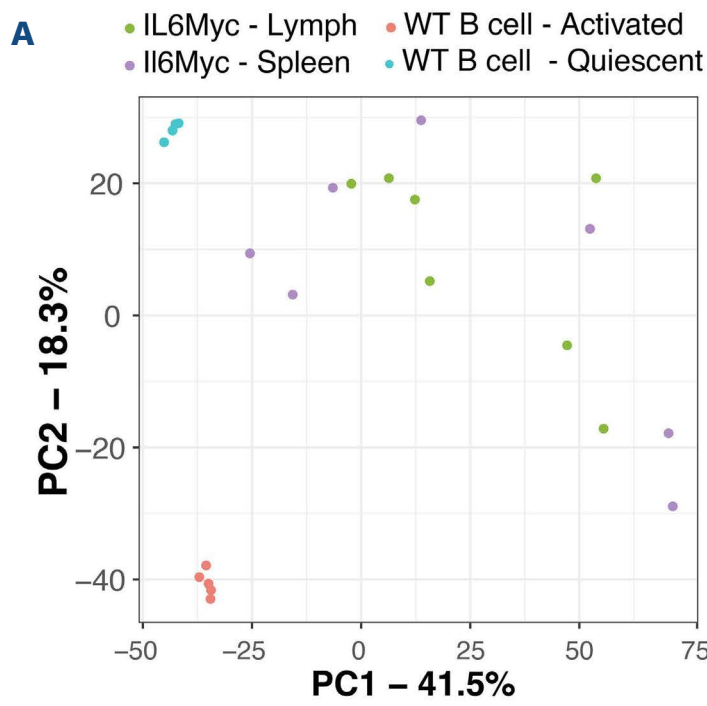
In order to determine which genes are differentially expressed in tumors we compared expression levels in all

IL6Myc tumors (SPL, MLN) to activated B cells, which are similar to normal plasma cells. About half of all expressed genes (9,713 vs. 18,551 total) were significantly differentially expressed ($q \leq 0.05$) in tumors compared to controls and strongly skewed toward increased expression (6,411 up vs. 3,302 down) (Figure 1C; IL6Myc_v_activated_b_DGE.xlsx). This pattern resembles other *Myc* overexpression studies¹⁹ and is indicative of a global change in gene expression. Under these circumstances, differential expression of individual genes could not be confidently discerned by conventional methods. Instead, we performed GSEA to identify patterns and genes and reverse-phase protein (RPPA) to validate misexpression of cancer-related proteins.

IL6Myc gene expression pattern is consistent with high-risk disease

In order to identify sets of genes associated with transformation and MM we performed GSEA, which is less sensitive to global changes because it compares rank order instead of expression levels of genes. Of the top 100 enriched gene sets (by normalized enrichment score) generated by comparing IL6Myc tumor and activated B cells, solid cancers ($n=22$), hematological malignancies ($n=13$), extracellular matrix gene sets ($n=16$), and stemness ($n=10$) were highly represented. Of solid cancers, gene sets from prostate and breast cancer were the most represented (Figure 1D; *Online Supplementary Table S1*). In order to identify which genes contribute to enrichment of these top gene sets, we performed leading edge analysis (*Online Supplementary Figure S3A, B*). This identified 274 genes that drove enrichment of >5 gene sets (*Online Supplementary Table S2*). We validated three of these genes by qPCR due to their association with oncogenesis in previous literature: *CLU*,²⁰ *CTSB*,²¹ and *TGFBI*.²² Although each was up-regulated as expected, none were significant due to high between sample variance (*Online Supplementary Figure S3C*).

Three MM gene sets were highly enriched; ZHAN_MULTIPLE_MYELOMA_MS_UP gene set, which is associated with high-risk MMSET (multiple myeloma SET domain)-activating translocations,²³ ZHAN_MULTIPLE_MYELOMA_CD1_DN, enrichment of which means IL6Myc is dissimilar to the low-risk CD-1 subtype; and ZHAN_MULTIPLE_MYELOMA_DOWN (Figure 1E). In order to validate these genes sets we performed qPCR in seven MLN tumors *versus* activated B-cell controls on the top two genes for each set identified by leading-edge analysis (*Online Supplementary Figure S3D*). qPCR validated upregulation of *CTS3* and *MITF* for the ZHAN_MULTIPLE_MYELOMA_MS_UP gene set. Although little is known about the role of either gene in MM, the IL6Myc model provides a system to test their role in myelomagenesis. However, neither gene (*DOK3*, *HES1*) for



Continued on following page.

Figure 1. IL6Myc tumors resemble human multiple myeloma. (A) Gene expression was measured by RNA sequencing (RNA-seq) for IL6Myc tumors and activated and quiescent wild-type (WT) B cells from BALB/c mice. Principle component analysis (PCA) was performed to determine the similarity between tumor origin (mesenteric lymph nodes or spleen) and type of B cell (activated or quiescent). (B) Comparison of the tumor types using PCA of RNA-seq gene expression data. Density plots for the PC of each tumor type are plotted on the X and Y axis. Centroids and error bars are indicated in tan, with a table indicating the distance between IL6Myc centroid and each cancer. (C) Volcano plot of differential expression comparing mesenteric lymph node tumor to activated B-cell (plasmablast) control by RNA-seq. Red indicates genes that are significantly ($q \leq 0.05$) differentially expressed, with no log₂ fold change cutoff. (D) Summary of the top 100 enriched gene sets from gene set enrichment analysis (GSEA) of IL6Myc tumors compared to activated B cells. (E) Top multiple myeloma gene sets from GSEA for IL6Myc tumor versus activated B cells. (F) Volcano plot of differential protein expression from RPPA of tumor versus normal B cells. Red; $P < 0.01$, no log₂ fold change cutoff. (G) Correlation of protein (RPPA) and RNA (RNA-seq) log₂ fold change for significantly differentially expressed genes/proteins comparing tumor versus normal B cells. Blue line, best fit linear regression ($r = 0.27$; $P \leq 0.001$). ALL: acute lymphoblastic leukemia; AML: acute myeloid leukemia; MM: multiple myeloma; DLBCL: diffuse large B-cell lymphoma.

ZHAN_MULTIPLE_MYELOMA_CD1_DN and only *ITGA2B* for the ZHAN_MULTIPLE_MYELOMA_DOWN were upregulated as expected. These data support that the gene expression patterns of IL6Myc tumors resemble MMSET and high-risk MM but lack other defining expression features.

In order to determine which oncoproteins are mis-expressed in IL6Myc tumors, and to validate expression by RNA-seq, we performed RPPA. When IL6Myc tumors were compared to WT splenic B cells isolated from BALB/c mice, 144 of the 333 proteins tested were differentially expressed ($P < 0.01$) (Figure 1F). In order to validate RNA-seq expression changes with RPPA, we performed linear regression analysis. This showed a modest, though significant correlation between expression patterns ($r = 0.27$; $P \leq 0.001$), with the expression a substantial subset correlating well (Figure 1G). Among correlating genes, three associated with MM were notable: *EPHA2* and *CD274* (up-regulated) and *STAT5A* (downregulated) (Figure 1G). *EPHA2* and *CD274* (PD-L1) are both targets of anti-MM therapy. Anti-*EPHA2* compounds are in clinical trials²⁴ and PD-L1 is a target for immunotherapy due to its success in other malignancies and elevated expression in relapse-refractory patients.²⁵ *STAT5A* decreases proliferation of MM cells and is a target for degradation of YTHDF2 which is upregulated in MM patients with poor outcomes.²⁶ These results show that IL6Myc tumors have features of poor prognosis MM and perhaps immune evasion.

Genes with fusions and mutations in IL6Myc tumors overlap with those in human multiple myeloma

The penetrance of MM in the IL6Myc mouse suggests that driving IL6 and Myc creates conditions for genetic lesions to arise that drive myelomagenesis. Because recurrent Ig fusions with non-Ig protein coding genes are a common feature of MM,²⁷ we used STAR-Fusion on the tumor RNA-seq datasets to identify 78 fusion genes in IL6Myc tumors. Excluding the intra-Ig rearrangements typical of B-lineage cells, 30 genes were involved in coding-coding (non-Ig protein-coding genes) fusions and the remaining ten were between Ig loci and other protein-coding genes. This ratio of coding-coding and Ig-coding is similar to human MM,

with normal B cells having fewer Ig-coding fusions per sample (Figure 2A; *Online Supplementary Table S3*). A significant ($P < 0.002$) number ($n = 10$) of the IL6Myc genes involved in fusions overlapped with genes involved in fusions identified in human MM from the MMRF data set (Figure 2B). One fusion, Snd1-Braf, was between the same two genes and is associated with several cancers²⁸⁻³⁰ (*Online Supplementary Table S3*). A more in-depth examination of fusions shared between IL6Myc and human MM may reveal a role in myelomagenesis.

In order to determine whether IL6Myc mice accumulate missense mutations in genes associated with Myc-driven MM, whole-exome sequencing (WES) was performed on 45 MLN whole-tumor samples. In order to eliminate background variation, WES was performed on five WT kidney samples from BALB/c mice and identified variants were subtracted. We eliminated other common variants using single-nucleotide polymorphism from the Mouse Genome Project. In order to ensure high-confidence variants that result in protein mutation, we considered only missense and nonsense mutations and used a baseline 5% allelic frequency, leaving 1,351 variant-containing genes (Figure 2C; *Online Supplementary Table S4*). This IL6Myc gene list overlapped significantly (324 of 1,351 genes; $P < 6.4 \times 10^{-22}$) with the most common human variants (top 1% of genes >10 variants human MM from the MMRF database; Figure 2D). Perhaps more importantly, a significant ($P < 0.0003$) number of IL6Myc variant-containing genes ($n = 12$) overlapped with the 80 genes with known driver mutations in human MM.³¹ This list included PIM1, which accumulated mutations in the kinase domain of the PIM1 gene in both IL6Myc tumors and in human MM (Figure 2E). Overall, these data show that IL6Myc tumors exhibit an accumulation of variants in many of the same genes with genetic lesions in human MM, suggesting that the IL6Myc mouse is able to acquire the many of same mutations that drive human MM.

Gene expression of IL6Myc cell lines resemble human multiple myeloma

We derived five cell lines from IL6Myc splenic (IL6Myc-1)

and mesenteric lymph node (IL6Myc2-5) tumors. Cell lines adapted readily to culture, with similar doubling times ranging from 33 (IL6Myc-3) to 48 h (IL6Myc-2,5) (Figure 3A; *Online Supplementary Figure S4A*). In order to determine their similarity to primary tumors and human MM, we performed RNA-seq and RPPA. The RNA expression profiles in IL6Myc cell lines were similar to each other but distinct from primary tumor and normal primary B cells

(*Online Supplementary Figure S4B, C*). However, comparison of the top 100 GSEA enriched sets between primary tumor and cell lines identified 17 overlapping gene sets (*Online Supplementary Table S5*) suggesting that although some expression patterns are maintained, IL6Myc cell lines and primary tumors are transcriptionally distinct. Protein expression levels were more similar between IL6Myc tumors and cell lines (*Online Supplementary Figure*

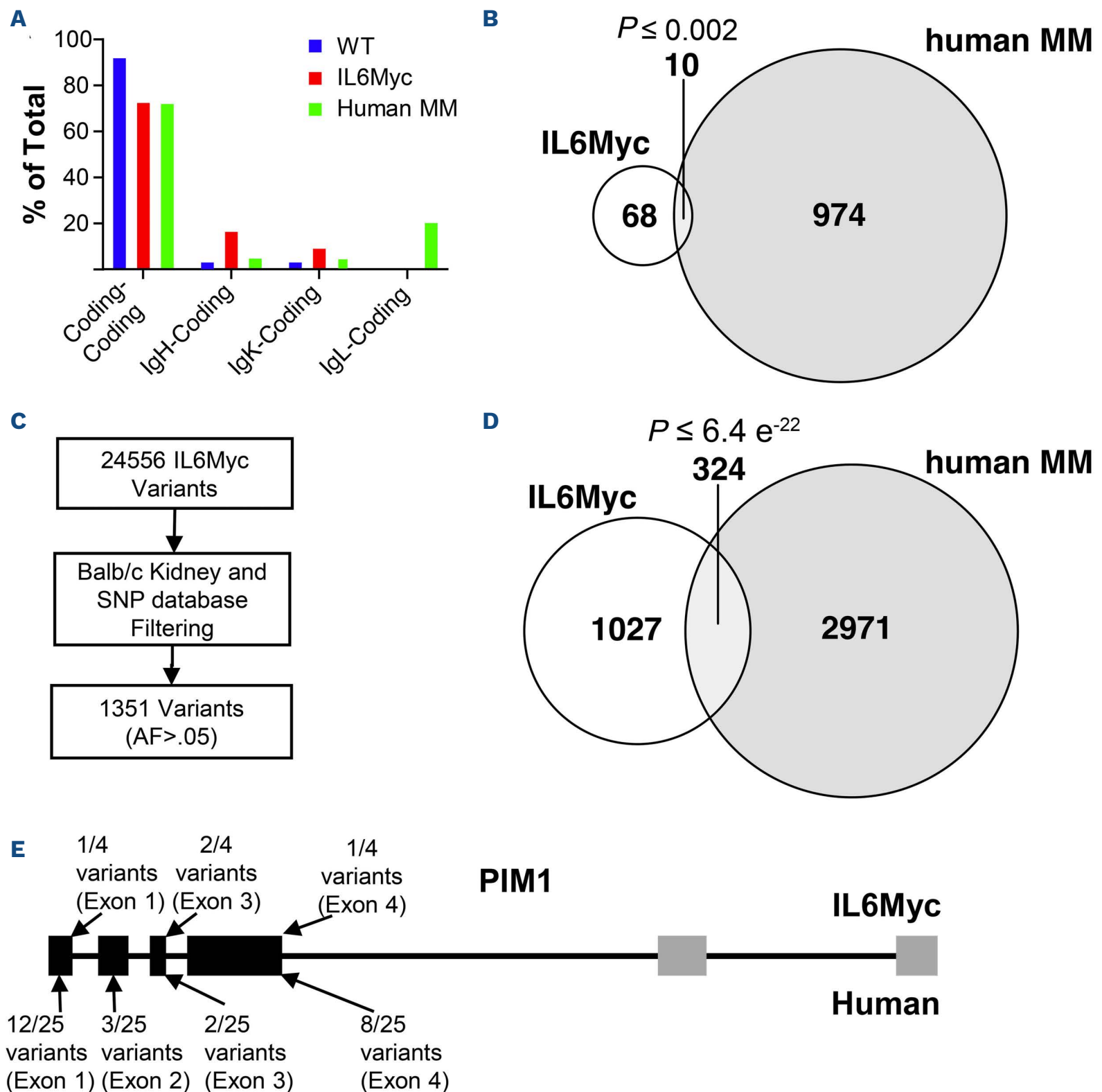
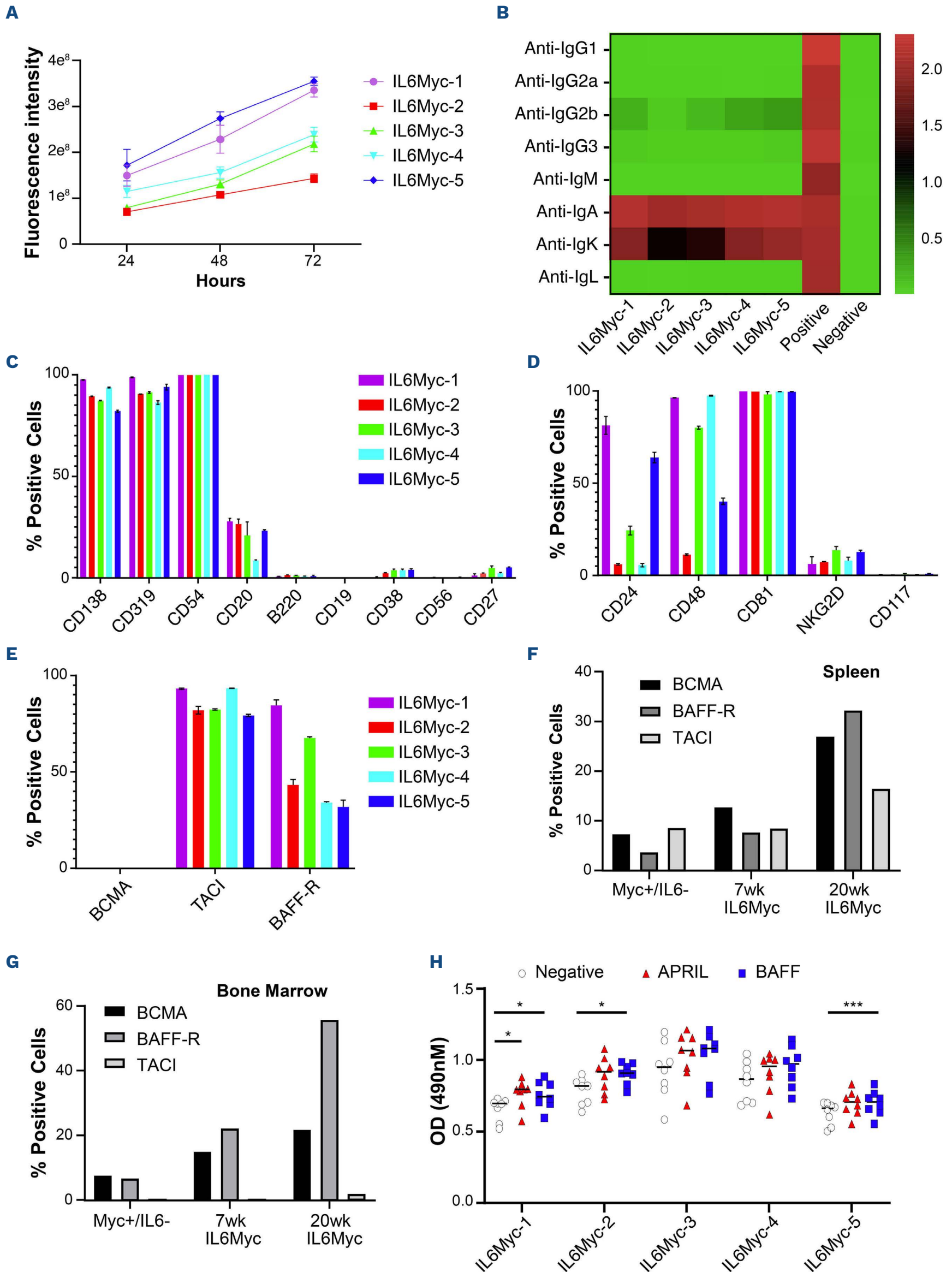


Figure 2. Genetic lesions in IL6Myc tumors significantly overlap with those observed in human multiple myeloma. (A) Gene fusions were identified in IL6Myc and wild-type (WT) B cells from RNA-sequencing (RNA-seq) data. Excluding inter-immunglobulin (Ig) rearrangements, most fusions were identified between non-Ig protein coding genes (coding-coding). Different from human multiple myeloma (MM), most Ig fusions were between the IgH locus and non-Ig protein coding genes. Blue: WT BALB/c B cells. Red: isolated B cells from IL6Myc tumors. Blue: fusions identified MM from RNA-seq data (ref). (B) Overlap of genes involved in fusions between IL6Myc MM (Multiple Myeloma Research Foundation [MMRF] data) is significant ($P \leq 0.002$). (C) Process for filtering variants. (D) Filtered variants identified by whole-exome sequencing in in IL6Myc ($N=1351$) overlap significantly ($N=324$; $P < 6.4e^{-22}$) with the top 1% most common variants identified from the MMRF database. (E) Variants from IL6Myc tumors (top) and the MMRF data set (bottom) were mapped onto the PIM1 gene. All variants localize to the N-terminal half. Statistical significance of overlap was determined by hypergeometric test (http://nemates.org/MA/progs/overlap_stats.html).



Continued on following page.

Figure 3. IL6Myc cell lines are IgA producing and have cell surface markers largely resembling human multiple myeloma. (A) Proliferation of IL6Myc cell lines measured by cell viability at 3 time points. (B) Immunglobulin (Ig) isotyping enzyme-linked immunorbant assay heatmap. Red indicates a higher signal, and green a weaker signal. Positive control Ig and negative control are indicated as “positive” and “negative”. Flow cytometry for the faction of cells staining positive for: (C) markers of clinical multiple myeloma (MM). Data was gathered in triplicate and error bars represent standard deviation. (D) Markers correlating with disease state in MM and/or those with value as immunotherapeutic targets. Data was gathered in triplicate and error bars represent standard deviation. (E) Survival and proliferation cell surface proteins in cell lines. Data was gathered in triplicate and error bars represent standard deviation. (F) Survival and proliferation cell surface proteins in mouse spleen. (G) Survival and proliferation cell surface proteins in bone marrow. (H) Growth of IL6Myc cell lines after 72 hours with addition of APRIL or BAFF compared to negative control. Significance was determined by *t* test. * $P < 0.05$; *** $P < 0.0001$. OD: optical density.

S4D), indicating that the cells lines are similar to the tumor. IL6Myc cell lines also most closely resembled human MM compared to other cancers (*Online Supplementary Figure S4E, F*). This indicates that despite differences in expression, the IL6Myc cell lines are similar to IL6Myc primary tumors and still model human MM.

IL6Myc cell lines resemble malignant plasma cells by surface markers

In order to subtype the IL6Myc cell lines we evaluated Ig isotype expression and cell surface markers. IL6Myc cell lines production of IgA antibodies outstripped other isotypes (Figure 3B). IgA-producing MM is the second most common form of MM, comprising approximately 20% of human MM and is associated with worse survival compared to the more common IgG-producing MM.³² IL6Myc cell lines were consistent with plasma cells, exhibiting surface expression of high CD138, CD54 and SLAMF7, low CD20,³³ and were negative for CD19 and B220. However, the cell lines lacked CD56, a marker of human malignant plasma cells (Figure 3C). Positive staining of CD24, a marker of MM stemness,³⁴ combined with CD81⁺CD117⁻, which correlates with high-risk disease, suggests that, despite the lack of CD56, IL6Myc cells resemble high-risk MM.³⁵

In order to evaluate whether IL6Myc cell lines contain targets for existing chimeric antigen receptor (CAR) T cells, we performed flow cytometry for CD48, NKG2D, and BCMA (Figure 3D, E). Variable, but positive, staining was observed for CD48 and NKG2D, but negative for BCMA. This contrasts with primary IL6Myc splenic tumors and bone marrow from IL6Myc mice which stained positive for cell surface BCMA (Figure 3F). It also contrasts with RNA-seq from the IL6Myc cell lines which shows low, but significant expression of BCMA at the mRNA level (*Online Supplementary Figure S5*), indicating that BCMA expression is post-transcriptionally regulated in IL6Myc cell lines. Thus, although tumors in intact IL6Myc mice would be useful for studying BCMA CAR-T therapies the cell lines are likely not (Figure 3F, G).

BCMA, BAFF-R, and TACI provide important survival and proliferative messages to B lineage cells, have shared ligands, and signal through similar pathways. BAFF-R is typically expressed early in plasma cell development, and then lost in favor of BCMA and TACI.^{36,37} Primary IL6Myc tumors from spleen and bone marrow (Figure 3F, G) express

all three, to varying degrees, but IL6Myc cell lines retaining only BAFF-R and TACI (Figure 3E). Although BAFF-R positivity has been noted in some subsets of MM, it is not a common feature.³⁸

These data suggest that BAFF-R and TACI may provide important survival and growth signals to IL6Myc cell lines. In order to test this, cell lines were stimulated with BAFF, a ligand of BAFF-R and TACI, or APRIL, a ligand of TACI and BCMA. Although BAFF ligand significantly ($P < 0.05$) stimulated growth of three of the five cell lines (IL6Myc1, 2, and 5) and APRIL only one (IL6Myc-1), a trend toward increased growth is evident for both ligands in all cell lines (Figure 3H). These results indicate that BAFF-R, and sometimes TACI, stimulate enhanced growth of IL6Myc cell lines while BCMA does not. These results also indicate that IL6Myc cell lines would be useful for testing the efficacy of CAR T cells targeting TACI and/or BAFF-R, which has been evaluated in conjunction with BCMA targeting in MM.³⁹ These targets may become more relevant in patients who relapse after BCMA targeted therapy and the approximately 5.7% of patients that are BCMA negative.⁴⁰

IL6Myc-1 cells home to the bone marrow and induce osteolytic disease

Particularly given their derivation (from splenic and mesenteric tumors), we sought to determine whether IL6Myc cell lines would serve as useful models by engrafting them into both immunocompromised (NOD-SCID) and immunocompetent (BALB/c) mice. We injected 2×10^6 cells intravenously (IV) into BALB/c mice following priming by lethal whole-body irradiation (10 Gy). Lethal host priming required hematopoietic stem cell rescue using bone marrow transplantation (3×10^6 cells). We also injected 2×10^6 cells IV into immunocompromised NOD-SCID mice without irradiation (Figure 4A). Several host mice developed hind limb paralysis suggesting plasma cell infiltration of the spine. Histopathological analysis of the spine showed extramedullary tumor growth that damaged spinal nerve roots and intramedullary tumor growth that compressed the spinal cord directly (Figure 4B). In order to test whether these mice develop myeloma-like bone disease (MBD), we completed μ CT analysis. This demonstrated severe bone loss in L2-4 spine in both BALB/c and NOD-SCID mice (Figure 4C, D). Changes in serum biomarkers of

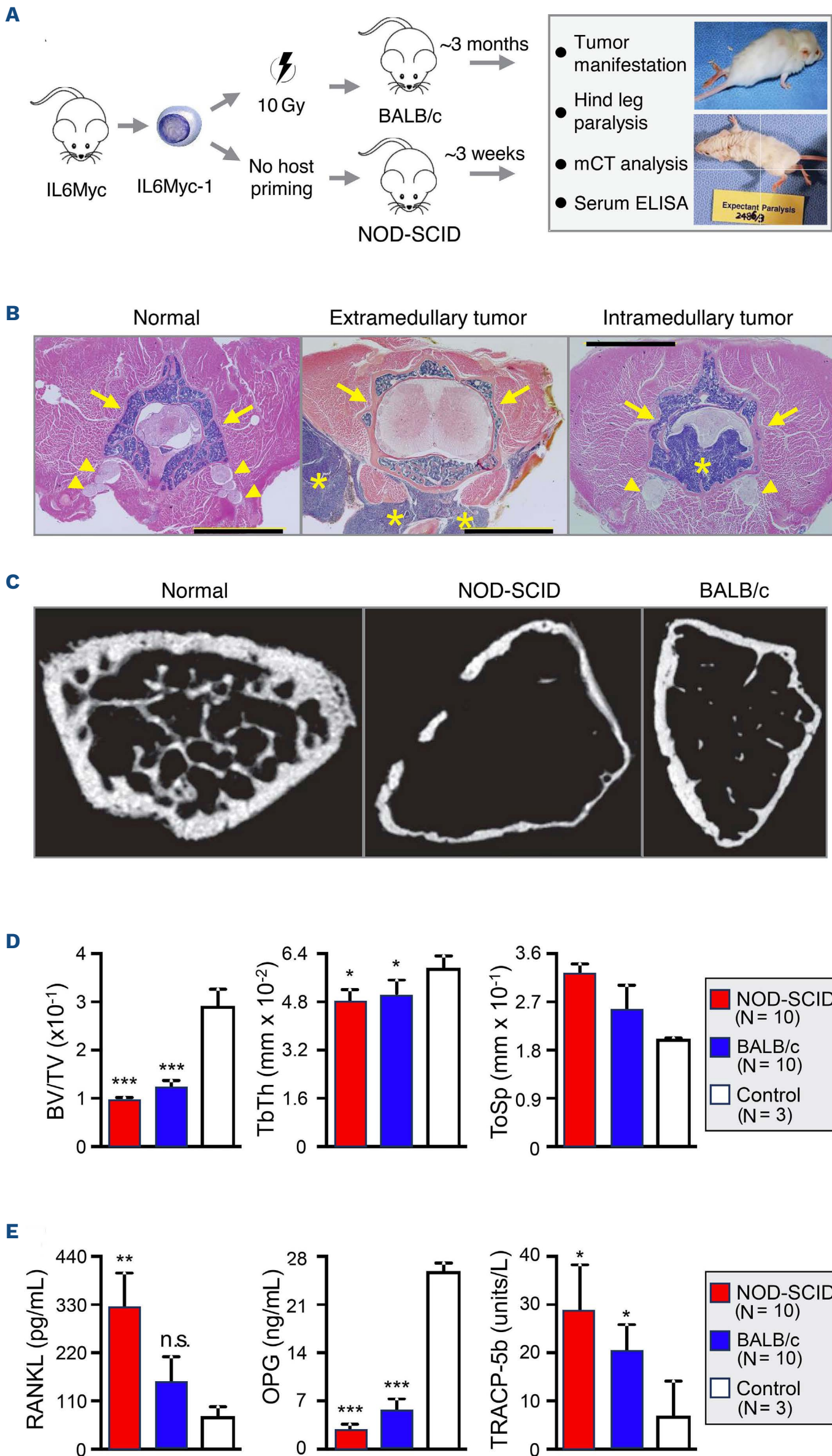


Figure 4. Osteolytic disease in IL6Myc-1 autografted host mice. (A) Study design. IL6Myc-1 cells were derived from the spleen of a PCT-bearing IL6Myc mouse. Two million tumor cells were transferred intravenously (IV) to lethally irradiated BALB/c mice rescued by co-transfer of hematopoietic stem cells obtained from untreated BALB/c mice (top). Adoptive transfer of IL6Myc-1 cells to untreated NOD-SCID mice was used as control (bottom). Tumor manifestation required ~3 months in BALB/c and ~3 weeks in NOD-SCID mice. More than half of the mice in both groups developed weakness or full-fledged paralysis of hind limbs indicated by 2 photographs on the right. (B) Two types of tumor growth (yellow asterisks) may underlie hind leg paralysis. Extramedullary tumor expansion (center panel) can damage spinal nerves and nerve roots but leaves vertebral bone (containing normal bone marrow) and spinal cord intact (yellow arrows). Intramedullary tumor expansion (right) can compress the spinal cord after destroying bone and infiltrating bone marrow (yellow arrows) but leaves spinal nerves (yellow arrowheads) unscathed. Transversal tissue sections stained according to hematoxylin & eosin in all 3 cases, including the normal mouse shown in the left panel. Black horizontal lines denote a scale of 2 mm. (C) Representative transversal X-ray microtomography (μ CT) images of the proximal femur from tumor-bearing NOD-SCID or BALB/c mice adoptively transferred with IL6Myc-1 cells. A normal femur used as control is shown for comparison. (D) Bar diagrams indicating bone loss in L2-4 spine of adoptively transferred BALB/c mice (blue) and NOD-SCID mice (red) compared to normal mice (white). (E) Bar diagrams indicating changes in serum biomarkers of osteolytic disease. Mean values and standard deviation of the mean are plotted (* $P < 0.05$; ** $P < 0.01$; *** $P < 0.001$). ELISA: enzyme-linked immunorbant assay; n.s.: not significant.

osteolytic disease were also higher in NOD-SCID than BALB/c hosts, e.g., soluble RANKL was twice as high (324 ± 78.5 vs. 152 ± 59.2 pg/mL) and OPG was twice as low (2.65 ± 0.972 vs. 5.73 ± 1.60 ng/mL). Soluble TRAP was also highest in NOD-SCID (28.5 ± 9.76 U/L) followed by BALB/c (20.4 ± 5.38 U/L) with both significantly elevated compared to controls (6.87 ± 7.24 U/L) (Figure 4E). These results suggest that IL6Myc-1 cells result in MM-like disease like that observed in transgenic mice and, importantly, homes to typical sites of MM in the bone marrow.

IL6Myc cell lines are resistant to dexamethasone

In order to determine how IL6Myc cell lines respond to commonly used MM pharmacological agents, we treated cell lines with bortezomib, dexamethasone, panobinostat, melphalan, and 4-hydroxyperoxy cyclophosphamide (activated cyclophosphamide). All cell lines were sensitive to bortezomib (Figure 5; *Online Supplementary Figure S6A, H*) and panobinostat (Figure 5; *Online Supplementary Figure S6D, H*), but only died with the highest concentrations of pomalidomide (Figure 5; *Online Supplementary Figure S6C, H*), melphalan (Figure 5; *Online Supplementary Figure S6E, H*) and 4-hydroxyperoxy cyclophosphamide (Figure 5; *Online Supplementary Figure S6F, H*). Cell lines were insensitive to dexamethasone, with >50% of cells surviving the highest

doses in three of five cell lines (Figure 5; *Online Supplementary Figure S6B, G, H*). The cell lines varied in their sensitivities to each drug, but largely followed similar drug response patterns. Resistance to pomalidomide treatment was expected due to its reduced activity in mice, but resistance to dexamethasone indicates that the IL6Myc cell lines are associated with aggressive, poor prognosis MM.⁴¹

Discussion

The results of comprehensive genomic analysis reflect the phenotypic observation that the IL6Myc mouse develops high-risk, aggressive MM. Phenotypically, the tumors in IL6Myc mice resemble human MM including bone marrow infiltrating malignant plasma cells, MM-like bone disease, serum M-spike, and spleen, MLN, peripheral lymph nodes, kidney, and liver involvement.¹²⁻¹⁴ Although RNA-seq data was challenging to interpret, there was some evidence from GSEA that IL6Myc tumors also resemble high-risk MM through enrichment of the high-risk MMSET gene set²³ (Figure 1). Protein expression analyses provided further evidence of high-risk disease including exclusive expression of IgA32 (Figure 3) reduced expression of STAT5 and increased expression of PD-L1, both of which are linked to increased dis-

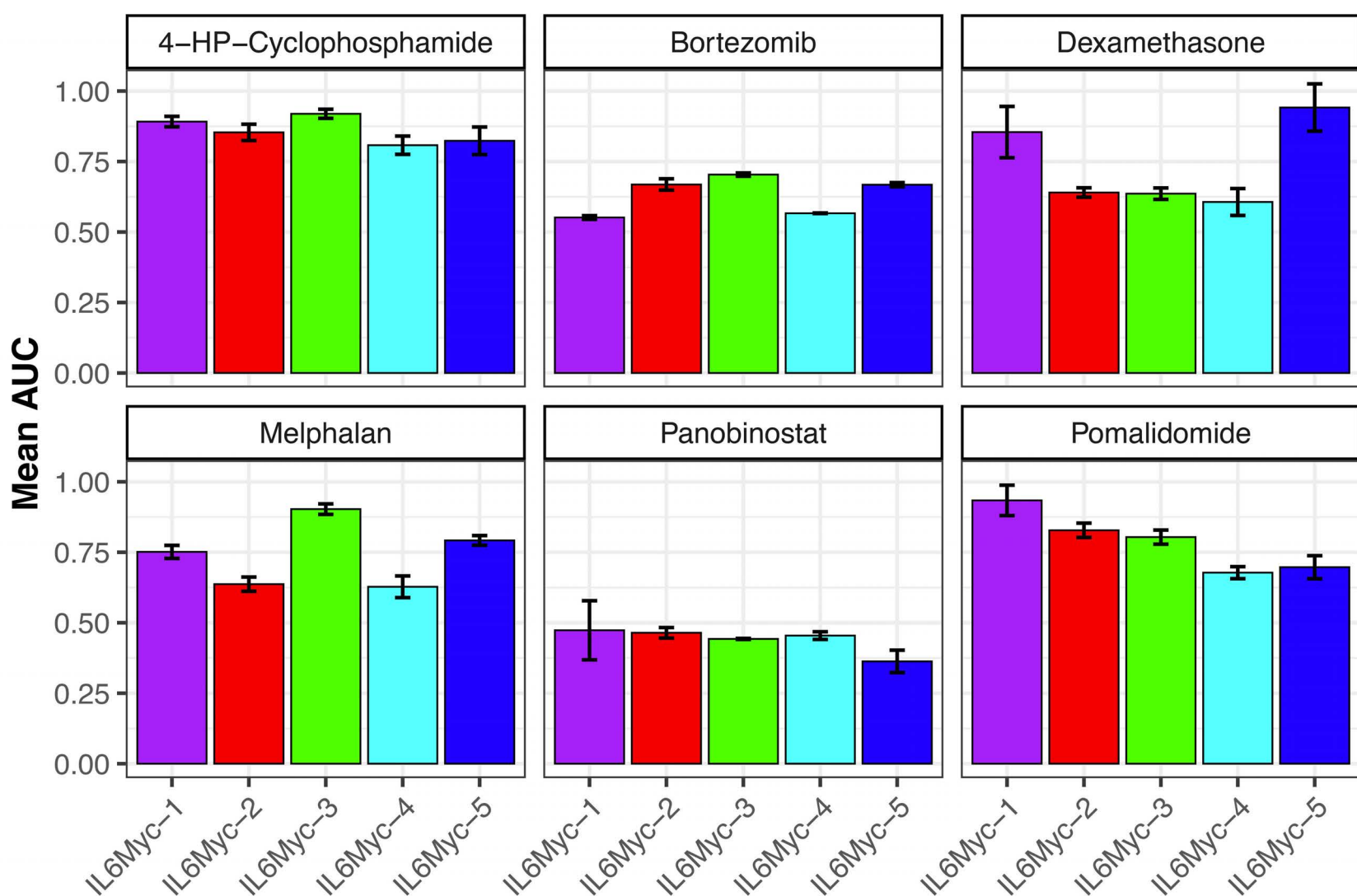


Figure 5. IL6Myc response to anti-multiple myeloma drugs. Summary of area under the curve (AUC) values of 4-hydroxyperoxy cyclophosphamide (4-HP-Cyclophosphamide), bortezomib, dexamethasone, melphalan, panobinostat, and pomalidomide. Data was collected in triplicate and error bars represent standard deviation.

ease severity in human MM^{25,26} (Figure 1). High-risk disease was also indicated by CD24, a marker of stemness,³⁴ and by CD81⁺CD117⁻, a diagnostic marker of poor prognosis MM³⁵ (Figure 3). Thus, the IL6Myc mouse tumors and cell lines have many of the molecular hallmarks of high-risk or aggressive MM.

The IL6Myc mouse is also a promising model for understanding the development of MM. Our data show an accumulation of variants and fusions in IL6Myc tumor genes that overlap significantly with genes, including transforming genes, with genetic lesions in human MM (Figure 2). This strongly suggests that IL6Myc mice favor acquisition of transforming mutations. The common location of IL6Myc and human MM variants in the kinase domain of PIM1 was particularly striking. PIM kinase inhibitors have shown promise in treatment of MM with several open clinical trials including in relapse/refractory MM.⁴² Although PIM2 is often upregulated in MM, inhibitors are pan-PIM kinase⁴² and may hit other PIM kinases. The IL6Myc mouse is a useful model to test the role of PIM1 and other PIM kinases in myelomagenesis and treatment.

IL6Myc mice are also useful for developing immunotherapies against MM. The tumors of intact mice display BCMA and are, therefore, useful in testing CAR T cells directed against this target. The IL6Myc cell lines do not display BCMA and are thus less useful in this regard.

However, IL6Myc cell lines allow study of how the BCMA, TACI and BAFF-R axis can be exploited to better treat MM. These receptors provide important proliferative and survival signals to MM cells. Although BCMA and TACI positivity is found in most forms of MM, BAFF-R positivity is less common. IL6Myc cell lines expressed cell surface TACI and surprisingly, BAFF-R. Stimulation experiments confirmed that BAFF-R, and likely TACI, can stimulate growth in IL6Myc cell lines while BCMA does not (Figure 3). This pattern mirrors non-remission patients who also express BAFF-R and TACI.⁴³ This expression pattern accommodates the high circulating BAFF levels found in MM that tend to increase with disease progression.⁴⁴ Immuno-targeting of BAFF-R and TACI would therefore be useful in BAFF-R⁺TACI⁺ MM. Indeed, recently developed CAR T cells displaying BAFF ligand can kill MM cells displaying BAFF-R, TACI, or BCMA.³⁹ Because of a paucity of BAFF-R-positive cell lines, IL6Myc cell lines and primary tu-

mors are uniquely poised to examine the role of BAFF-R in MM both *in vitro* and, due to their homing patterns (Figure 4), *in vivo*. Further studies of these receptors in IL6Myc may elucidate novel therapies on this axis that otherwise would be difficult to address in other MM cell lines.

Disclosures

No conflicts of interest to disclose.

Contributions

MDP was involved in research design, collected, and analyzed data, and assisted in writing the paper. FS, YC, VZ and XJ collected and analyzed data, and derived IL6Myc cell lines. RS, JA, MTZ and AM analyzed data, performed bioinformatics work, and assisted in writing the paper. SJ was involved in research design, analyzed data, and helped to write the paper. DP helped to analyze data and to write the paper. MP oversaw the work, analyzed data, and helped to design and to write the paper.

Acknowledgements

Thank you to the Linda T. and John A. Mellows Center for Genomic Sciences and Precision Medicine at the Medical College of Wisconsin for help with STAR-fusion and cell line RNA sequencing. Thank you to the University of Iowa Genomics division for primary tumor RNA sequencing. Thank you to Dr. Michael Tomasson, who helped us to get to core questions in the manuscript, and to Dr. Gail Bishop who provided support reviewing the paper.

Funding

SJ was supported by NCI R01CA151354; the William G. Schuett, Jr., Multiple Myeloma Research Endowment; and a generous gift from the Riney Family Multiple Myeloma Research Initiative. MAP was supported by a grant from the Aiming for a Cure Foundation.

Data-sharing statement

The authors are committed to open sharing of data. All sequencing data has been deposited in the Gene Expression Omnibus (<https://www.ncbi.nlm.nih.gov/geo/>, accession number: GSE220828). All other data will be provided upon request to the corresponding author.

References

- Majithia N, Rajkumar SV, Lacy MQ, et al. Early relapse following initial therapy for multiple myeloma predicts poor outcomes in the era of novel agents. *Leukemia*. 2016;30(11):2208-2213.
- Teoh PJ, Chng WJ. CAR T-cell therapy in multiple myeloma: more room for improvement. *Blood Cancer J*. 2021;11(4):84.
- Yamamoto L, Amodio N, Gulla A, Anderson KC. Harnessing the immune system against multiple myeloma: challenges and opportunities. *Front Oncol*. 2020;10:606368.
- Chesi M, Robbiani DF, Sebag M, et al. AID-dependent activation of a MYC transgene induces multiple myeloma in a conditional mouse model of post-germinal center malignancies. *Cancer Cell*. 2008;13(2):167-180.
- Croese JW, Vas Nunes CM, Radl J, van den Enden-Vieveen MH, Brondijk RJ, Boersma WJ. The 5T2 mouse multiple myeloma model: characterization of 5T2 cells within the bone marrow. *Br J Cancer*. 1987;56(5):555-560.
- Hong S, Qian J, Yang J, Li H, Kwak LW, Yi Q. Roles of idiotype-specific t cells in myeloma cell growth and survival: Th1 and CTL

- cells are tumoricidal while Th2 cells promote tumor growth. *Cancer Res.* 2008;68(20):8456-8464.
7. Hallett WH, Jing W, Drobyski WR, Johnson BD. Immunosuppressive effects of multiple myeloma are overcome by PD-L1 blockade. *Biol Blood Marrow Transplant.* 2011;17(8):1133-1145.
 8. Guillerey C, Ferrari de Andrade L, Vuckovic S, et al. Immunosurveillance and therapy of multiple myeloma are CD226 dependent. *J Clin Invest.* 2015;125(5):2077-2089.
 9. Calcinotto A, Brevi A, Chesi M, et al. Microbiota-driven interleukin-17-producing cells and eosinophils synergize to accelerate multiple myeloma progression. *Nat Commun.* 2018;9(1):4832.
 10. Vanderkerken K, Asosingh K, Croucher P, Van Camp B. Multiple myeloma biology: lessons from the 5TMM models. *Immunol Rev.* 2003;194:196-206.
 11. Croucher DC, Richards LM, Tsofack SP, et al. Longitudinal single-cell analysis of a myeloma mouse model identifies subclonal molecular programs associated with progression. *Nat Commun.* 2021;12(1):6322.
 12. Rutsch S, Neppalli VT, Shin DM, et al. IL-6 and MYC collaborate in plasma cell tumor formation in mice. *Blood.* 2010;115(9):1746-1754.
 13. Duncan K, Rosean TR, Tompkins VS, et al. (18)F-FDG-PET/CT imaging in an IL-6- and MYC-driven mouse model of human multiple myeloma affords objective evaluation of plasma cell tumor progression and therapeutic response to the proteasome inhibitor ixazomib. *Blood Cancer J.* 2013;3(11):e165.
 14. Sun F, Cheng Y, Walsh SA, et al. Osteolytic disease in IL-6 and Myc dependent mouse model of human myeloma. *Haematologica.* 2020;105(3):e111-e115.
 15. Sher T, Miller KC, Deeb G, Lee K, Chanan-Khan A. Plasma cell leukaemia and other aggressive plasma cell malignancies. *Br J Haematol.* 2010;150(4):418-427.
 16. Chng WJ, Huang GF, Chung TH, et al. Clinical and biological implications of MYC activation: a common difference between MGUS and newly diagnosed multiple myeloma. *Leukemia.* 2011;25(6):1026-1035.
 17. Holien T, Vatsveen TK, Hella H, Waage A, Sundan A. Addiction to c-MYC in multiple myeloma. *Blood.* 2012;120(12):2450-2453.
 18. Parashar D, Geethadevi A, Aure MR, et al. miRNA551b-3p activates an oncostatin signaling module for the progression of triple-negative breast cancer. *Cell Rep.* 2019;29(13):4389-4406.
 19. Nie Z, Hu G, Wei G, et al. c-Myc is a universal amplifier of expressed genes in lymphocytes and embryonic stem cells. *Cell.* 2012;151(1):68-79.
 20. Ming X, Bao C, Hong T, et al. Clusterin, a novel DEC1 target, modulates DNA damage-mediated cell death. *Mol Cancer Res.* 2018;16(11):1641-1651.
 21. Cheriya V, Kuhns MA, Kalaycio ME, Borden EC. Potentiation of apoptosis by histone deacetylase inhibitors and doxorubicin combination: cytoplasmic cathepsin B as a mediator of apoptosis in multiple myeloma. *Br J Cancer.* 2011;104(6):957-967.
 22. Kaiser MF, Johnson DC, Wu P, et al. Global methylation analysis identifies prognostically important epigenetically inactivated tumor suppressor genes in multiple myeloma. *Blood.* 2013;122(2):219-226.
 23. Zhan F, Huang Y, Colla S, et al. The molecular classification of multiple myeloma. *Blood.* 2006;108(6):2020-2028.
 24. Wilson K, Shiuan E, Brantley-Sieders DM. Oncogenic functions and therapeutic targeting of EphA2 in cancer. *Oncogene.* 2021;40(14):2483-2495.
 25. Tamura H, Ishibashi M, Sunakawa-Kii M, Inokuchi K. PD-L1-PD-1 Pathway in the Pathophysiology of Multiple Myeloma. *Cancers (Basel).* 2020;12(4):924.
 26. Hua Z, Wei R, Guo M, et al. YTHDF2 promotes multiple myeloma cell proliferation via STAT5A/MAP2K2/p-ERK axis. *Oncogene.* 2022;41(10):1482-1491.
 27. Cleynen A, Szalat R, Kemal Samur M, et al. Expressed fusion gene landscape and its impact in multiple myeloma. *Nat Commun.* 2017;8(1):1893.
 28. Chu YH, Wirth LJ, Farahani AA, et al. Clinicopathologic features of kinase fusion-related thyroid carcinomas: an integrative analysis with molecular characterization. *Mod Pathol.* 2020;33(12):2458-2472.
 29. Jang JS, Lee A, Li J, et al. Common oncogene mutations and novel SND1-BRAF transcript fusion in lung adenocarcinoma from never smokers. *Sci Rep.* 2015;5:9755.
 30. Klubickova N, Agaimy A, Hajkova V, et al. RNA-sequencing of myxoinflammatory fibroblastic sarcomas reveals a novel SND1::BRAF fusion and 3 different molecular aberrations with the potential to upregulate the TEAD1 gene including SEC23IP::VGLL3 and TEAD1::MRTFB gene fusions. *Virchows Arch.* 2022;481(4):613-620.
 31. Oben B, Froyen G, Maclachlan KH, et al. Whole-genome sequencing reveals progressive versus stable myeloma precursor conditions as two distinct entities. *Nat Commun.* 2021;12(1):1861.
 32. Nair B, Waheed S, Szymonifka J, Shaughnessy JD, Jr., Crowley J, Barlogie B. Immunoglobulin isotypes in multiple myeloma: laboratory correlates and prognostic implications in total therapy protocols. *Br J Haematol.* 2009;145(1):134-137.
 33. Ajaz B, Akhtar A, Chang CC, Solh M, Tangonan K, Khaled Y. Plasma cell CD20 expression: primary aberrant expression or receptor up-regulation. *Leuk Lymphoma.* 2014;55(2):444-446.
 34. Gao M, Bai H, Jethava Y, et al. Identification and characterization of tumor-initiating cells in multiple myeloma. *J Natl Cancer Inst.* 2020;112(5):507-515.
 35. Chen F, Hu Y, Wang X, Fu S, Liu Z, Zhang J. Expression of CD81 and CD117 in plasma cell myeloma and the relationship to prognosis. *Cancer Med.* 2018;7(12):5920-5927.
 36. Kampa M, Notas G, Stathopoulos EN, Tsapis A, Castanas E. The TNFSF Members APRIL and BAFF and their receptors TACI, BCMA, and BAFFR in oncology, with a special focus in breast cancer. *Front Oncol.* 2020;10:827.
 37. Lee L, Bounds D, Paterson J, et al. Evaluation of B cell maturation antigen as a target for antibody drug conjugate mediated cytotoxicity in multiple myeloma. *Br J Haematol.* 2016;174(6):911-22.
 38. Novak AJ, Darce JR, Arendt BK, et al. Expression of BCMA, TACI, and BAFF-R in multiple myeloma: a mechanism for growth and survival. *Blood.* 2004;103(2):689-694.
 39. Wong DP, Roy NK, Zhang K, et al. A BAFF ligand-based CAR-T cell targeting three receptors and multiple B cell cancers. *Nat Commun.* 2022;13(1):217.
 40. Salem DA, Maric I, Yuan CM, et al. Quantification of B-cell maturation antigen, a target for novel chimeric antigen receptor T-cell therapy in Myeloma. *Leuk Res.* 2018;71:106-111.
 41. Xu J, Su Y, Xu A, et al. miR-221/222-mediated inhibition of autophagy promotes dexamethasone resistance in multiple myeloma. *Mol Ther.* 2019;27(3):559-570.
 42. Wu J, Chu E, Kang Y. PIM kinases in multiple myeloma. *Cancers (Basel).* 2021;13(17):4304.
 43. Pan J, Sun Y, Zhang N, et al. Characteristics of BAFF and APRIL factor expression in multiple myeloma and clinical significance. *Oncol Lett.* 2017;14(3):2657-2662.
 44. Alexandrakis MG, Roussou P, Pappa CA, et al. Relationship between circulating BAFF serum levels with proliferating markers in patients with multiple myeloma. *Biomed Res Int.* 2013;2013:389579.